by medium porosity fritted glass. A silver wire coated with AgCl, employed as the pseudo-reference electrode, was separated from the working electrode by a fine fritted glass. $LiClO_4$ (0.2 M) was used as supporting electrolyte. Potentials were measured relative to an internal ferrocene ($E_{1/2}$ = 510 mV versus SCE) or anthracene ($E_{1/2}$ = -1.94 V versus SCE) standard. Cyclic voltammograms were recorded with a BAS-100 or a PAR 173 potentiostat driven by a PAR 175 Universal programmer.

Preparation of the Dianion Solutions. The acid (10 mmol), dissolved in THF, was slowly added to a 1 M LDA solution (20 mL) diluted with 12 mL of THF. The reaction mixture was stirred at room temperature for 3 to 5 h, and the solvent was evaporated under vacuum, yielding the solid dianion as a powder. A stock solution (0.3 M) was prepared by dissolution of the dianion in THF.

Where possible, the dianions were also prepared amine-free by deprotonation with butyllithium. Since identical results were attained with and without amine bases, we infer that the procedure for evaporative removal of diethylamine effectively produced free lithium salts uncomplicated by amine complexation effects described previously.[27,28]

Diphenylacetic acid was directly deprotonated with 2 equiv of *n*-butyllithium at 0 °C in THF. Phenylacetic acid was also directly metalated with *n*-butyllithium at -78 °C (slow addition); the reaction mixture was then allowed to warm to room temperature.

All the dianion solutions were very stable at room temperature in the presence of HMPA. Yellow octahedral crystals of dilithiated diphenylacetic acid were obtained after deprotonation of 2 mmol acid in 6 mL of THF with 4 mmol *n*-butyllithium (2.5 M) by maintaining the solution at -20 °C for 2 days.

In all cases, chemical trapping and characterization of alkylated products (isolated in ≥90% yield) derived from the dianions verified that the dianions indeed were formed under these conditions, as has been previously reported by others.[19,29] Although the dianions attack THF at elevated temperatures, no decomposition (as adjudged by yield of alkylation product) occurred at temperatures below 40 °C within the several hours necessary for these experiments.

The pale yellow color observed in these experiments is routinely observed when LDA is used as a base.[10] It is caused by the reaction of LDA with THF since no substrate decomposition product is observed after quenching the dianion solution. The colored product has no influence on the dianion cyclic voltammetry since scans of dianions prepared from LDA or from BuLi were identical. For example, the same electrochemical behavior was observed for the dianion of phenylthioacetic acid prepared in situ by this method and that purified by recrystallization of the dilithium salt.

The milky viscous appearance of the dilithiated alkanoic acids is attributed to strong aggregation rather than to formation of LiOH.[10] Aggregation proved to be a complication for obtaining ^{13}C NMR spectra because of the high substrate concentrations involved in those experiments, whereas cyclic voltammograms were obtained at much lower concentrations where aggregation was not significant.

pK_a Determination. (1) Equilibrium measurements: 1 mmol of the dilithiated acid (I) in 5 mL of THF/HMPA (4:1) was added to 1 mmol of the lithium carboxylate (II). The solution was stirred at room temperature. After 1 h, a homogeneous solution was generally formed, and the solution was stirred for 20 more h. The solution was then quickly cooled to -78 °C, and CD_3COOD (1 mL) was added to the reaction mixture. The usual workup gave the partially deuteriated acid. The deuterium content for each compound was determined by proton NMR, ^{13}C NMR, and mass spectroscopy. The equilibrium constant was always determined by approaching the equilibrium from both sides.

(2) Control experiments: The lithium carboxylate was dissolved in 5 mL of THF/HMPA (4:1) before addition of the dianion. The resulting solution was stirred for 3 min at room temperature before quenching as previously described at -78 °C.

Equilibration with triphenylmethane as indicator was accomplished in similar fashion, with triphenylmethane replacing the carboxylate salt II.

Acknowledgment. We are grateful to the National Science Foundation and the Robert A. Welch Foundation for support of this work.

(27) Ashby, E. C.; Argyropoulos, J. N. *Tetrahedron Lett.* **1984**, *25*, 7.
(28) Eleveld, M. B.; Hogeveen, H. *Tetrahedron Lett.* **1986**, *27*, 631.
(29) Creger, P. L. *J. Am. Chem. Soc.* **1967**, *89*, 2500.

Laser-Induced Fluorescence, Far-Infrared Spectroscopy, and Luminescence Quenching of Europium Zeolite Y: Site-Selective Probes of Extraframework Cations

Mark D. Baker,*,† Michael M. Olken,‡ and Geoffrey A. Ozin*

Contribution from the Lash Miller Chemistry Laboratories, Chemistry Department, University of Toronto, Toronto M5S 1A1, Canada. *Received August 17, 1987*

Abstract: In this paper, the far-infrared and laser-induced fluorescence spectra of ion-exchanged, dehydrated europium zeolite Y are reported. Both techniques indicate that europium ions locate in three major sites. The appearance of bands due to parity-forbidden transitions in the fluorescence spectra indicates that the local symmetry of these sites is either C_s, C_n, or C_{nv}. The migration of europium ions between these sites was observed following oxidation of the zeolite at 400 °C. The luminescence intensity was quenched by oxygen, obeying Stern-Volmer kinetics. The spectra recorded in the presence of oxygen indicate that the quenching is site selective. The recognition of molecules entering the pore system of the zeolite by an optical response is one of the goals of this study.

1. Introduction

Zeolite molecular sieves currently play an indispensable role in many technologically and economically important applications. Of primary importance are their uses as acidic cracking catalysts,[1] builders in detergents,[2] and fillers in the paper industry.[3] In the past 5-10 years, the characterization of these materials has become increasingly crucial to their future development in many new

†Current address: Chemistry Department, University of Guelph, Guelph, Ontario, Canada.
‡Current address: Central Research Catalysis Laboratory, Dow Chemical Co., Midland, MI 48674.

(1) Haynes, H. W. *Catal. Rev. Sci. Eng.* **1978**, *17*, 273. Gallezot, P. *Catal. Rev. Sci. Eng.* **1979**, *20*, 121.
(2) Llenado, R. A. *Proceedings of the Sixth International Zeolite Conference*, Reno, NV, July 1983, p 940.
(3) Quanchang, Z.; Minqdi, S.; Changlu, D.; Huari, Y.; Qixing, Z.; Zhiguo, Z. In *Zeolites: Synthesis, Structure, Technology and Application*; Hocevar, S., Pejovnik, S., Eds.; Elsevier: Amsterdam, 1985. Sersdale, R. Plenary Lecture.

0002-7863/88/1510-5709$01.50/0 © 1988 American Chemical Society

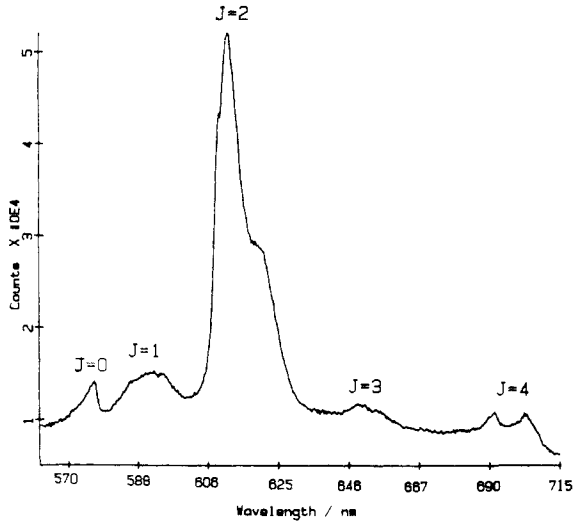

Figure 1. Laser-induced fluorescence spectrum of europium zeolite Y dehydrated at 400 °C. The transitions originate from the $^5D_0$ level and terminate at the ^7F_J levels indicated on the figure.

suggested areas.[4] To this end the development of many spectroscopic techniques specifically tailored to zeolite characterization has occurred. For example, recent advances in EXAFS,[5] solid-state NMR,[6] neutron and X-ray diffraction,[7] far-IR,[8] EPR,[9] and luminescence techniques[10] have, in combination, enormously widened the understanding of these materials.

The rare earth ion exchanged zeolites are well-known for their use as industrial catalysts in, for example, isomerization, alkylation, and cracking of hydrocarbons. The economic importance of these reactions has indeed stimulated much research on these materials aimed at improving and understanding these processes.[11] The rare earths have also been extensively studied in terms of their fluorescence properties and have been used in solid-state lasers and masers.[12-14]

In this paper we present the laser-induced fluorescence and far-IR spectra of europium zeolite Y. The luminescence data confirm earlier EPR studies of Brodbeck and Iton[15] and Iton et al.[16] that the zeolite provides a glassy environment for the guest ions. The optical techniques point to the europium ions locating in three major sites. In the absence of any diffraction data in the open literature on europium(III) zeolite Y or any site-specific cation information, this is the first data of its kind. One of the aims of this study is an investigation of optical responses to the intrusion of molecules into the pore system of the zeolite.

2. Experimental Section

Europium ion exchanged zeolite Y was prepared from ammonium zeolite Y ($Na_7(NH_4)_{49}Y$; Si/Al = 2.5). The starting material for this synthesis was sodium zeolite Y obtained from Union Carbide (lot no. 12074-33). Aqueous ion exchange was achieved under reflux for 2 days using 0.01 M europium chloride solution. After the product was washed free of chloride, the zeolite was stored over saturated ammonium chloride solution prior to spectroscopic examination. In all cases the dehydration was effected in situ by means of a slow temperature ramp to 400 °C at pressures better than 10^{-5} Torr. The temperature needed for removing various types of bound water are well documented in the zeolite literature.[36] Oxidation was performed by exposing the zeolite to a static pressure of 300 Torr of oxygen (Matheson ultrahigh purity) at 400 °C overnight. For the purposes of these experiments the zeolite powders were formed into self-supporting wafers using an applied pressure of 8 tonnes per cm^2.

Laser-induced fluorescence spectra were recorded with a Jobin-Yvon Ramanor monochromator and Instruments SA photon-counting system. The probe laser beam was supplied from a Coherent Radiation Innova 90-5 argon ion laser operating at 351.1 nm. Post-monochromatization was achieved with a Spex Lasermate. The far-IR spectra were recorded with a Nicolet 20F spectrometer using an in situ cell[17] at 4-cm^{-1} resolution. All the spectra described in this paper were recorded at room temperature. The samples were investigated in situ so that pre- and post-treatments could be performed without exposing the samples to air. In the laser-induced fluorescence experiments this had the added advantage of ensuring that the laser beam impinged on exactly the same part of the sample for each spectrum that was recorded. No deleterious effects on the samples due to the laser irradiation were evident in these experiments.

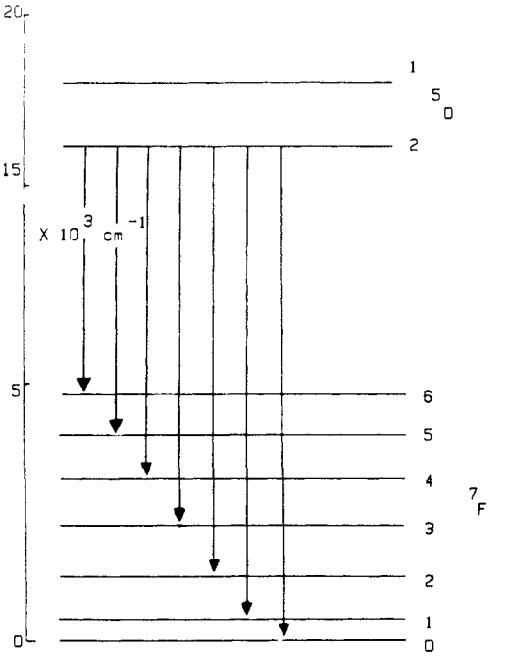

Figure 2. Electronic energy levels and fluorescence transitions for Eu^{3+}.

Table I. Relative Intensities (RI) and Bandwidths (BW (fwhm/cm^{-1})) for $^5D_0$ Emission from Europium Ions in Various Glassy Supports and Zeolite Y

transition assigt	phosphate		germanate		zeolite Y	
	BW	RI	BW	RI	BW	RI
$J = 0$	119	0.036	149	0.110	125	0.33
$J = 1$	313	1.000	342	1.000	500	1.00
$J = 2$	289	3.000	159	6.666	250	4.38
$J = 3$	234	0.219	282	0.260	200	0.49
$J = 4$	142	1.026	131	0.497	150	0.44

3. Results and Discussion

(A) Dehydrated Europium Zeolite Y: Site Information. The laser-induced fluorescence spectrum of EuY is shown in Figure 1. The ground electronic configuration of Eu(III) is f^6, and it is the transitions within the f orbitals that are responsible for the

(4) Ozin, G. A.; Godber, J.; Baker, M. D., *Studies in Surface Science and Catalysis*; Ward, J. W., Ed.; *Catalysis 1987*; Elsevier: New York, 1988; p 867. *Proceedings of the Xth North American Meeting of the Catalysis Society. Modern Spectroscopic Techniques*, May 17-22, 1987, San Diego, CA.

(5) Stucky, G. D.; Iton, L.; Morrison, T.; Shenoy, G.; Suib, S.; Zerger, R. P. *J. Mol. Catal.* **1984**, *27*, 71-80. Suib, S.; Zerger, R. P.; Morrison, T. I.; Shenoy, G. K. *J. Chem. Phys.* **1984**, *80*, 2203.

(6) Thomas, J. M.; Klinowski, J. *Adv. Catal.* **1985**, *33*, 199.

(7) Newsam, J. M.; Vaughan, D. E. *Zeolites: Synthesis, Structure, Technology and Application*; Drzaj, B., Hocevar, S., Pejovnik, S., Eds.; Elsevier: Amsterdam, 1985.

(8) Baker, M. D.; Ozin, G. A.; Godber, J. *J. Am. Chem. Soc.* **1985**, *107*, 3033. Ozin, G. A.; Godber, J. *J. Phys. Chem.* **1988**, *92*, 2841.

(9) Kevan, L. *Acc. Chem. Res.* **1987**, *20*, 1.

(10) Tanguay, J. F.; Suib, S. L. *Catal. Rev. Sci. Eng.* **1987**, *29*, 1.

(11) Eberly, P. E.; Kimberlin, C. N. *Adv. Chem. Ser.* **1971**, *102*, 374.

(12) Jansen, M.; Dunn, B.; Yang, D. L.; Farrington, G. *Opt. Lett.* **1984**, *10*, 119.

(13) Kaiser, W.; Garrett, C. G. B.; Wood, D. L. *Phys. Rev.* **1961**, *123*, 766.

(14) Grescovich, C.; Chernoch, J. P. *J. Appl. Phys.* **1974**, *45*, 4495.

(15) Brodbeck, C. M.; Iton, L. E. *J. Chem. Phys.* **1985**, *83*, 4285.

(16) Iton, L. E., Brodbeck, C. M.; Suib, S. L.; Stucky, G. D. *J. Chem. Phys.* **1983**, *79*, 1185.

(17) Baker, M. D.; Ozin, G. A.; Godber, J. *Catal. Rev. Sci. Eng.* **1985**, *27*, 591.

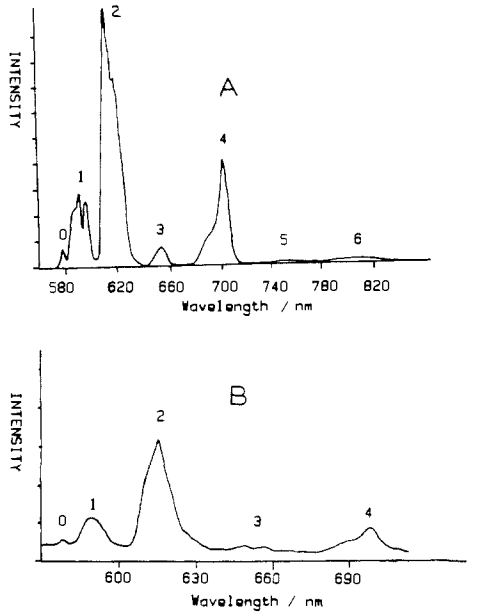

Figure 3. (A) Eu^{3+} luminescence in borosilicate glass (reprinted with permission from ref 18). (B) Eu^{3+} luminescence in porous Vycor glass (reprinted with permission from ref 19).

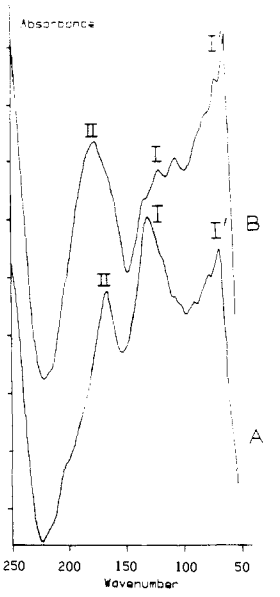

Figure 4. Far-IR spectra of Eu^{3+} zeolite Y: (A) dehydrated in vacuo at 400 °C; (B) oxidized at 400 °C under 300 Torr of oxygen. The spectra were recorded at room temperature. Note the relative growth and decay of europium ions located in sites II and I, respectively.

fluorescence. These transitions are forbidden by the electric dipole parity selection rule (Laporte's rule) in the free ion. However, in the solid state the local symmetry of the emitting europium ion is such that forced electric dipole transitions occur as a consequence of the coupling of odd electronic wave functions due to the odd-parity terms in the crystal field expansion. In this case the principal emission intensity is from the $^5D_0$ first excited state to the ground ^7F_J levels. Any emission intensity from the $^5D_1$ level was not observed in these experiments. The electronic energy level diagram appropriate for Eu^{3+} is shown in Figure 2.

The general appearance of the spectrum immediately alerts one to the "glassy" nature of the zeolite host. For comparison purposes, the fluorescence spectra of Eu^{3+} ions in borosilicate[18] and porous Vycor glass hosts[19] are shown in Figure 3. The relative intensities and bandwidths are similar in all three cases. Also, in comparison to the bandwidths observed for Eu^{3+} ions in single crystals,[18] which are a few wavenumbers, the bands are extremely broad (see Table I). Optical and fluorescence line-narrowing studies[20-23] have confirmed that in glasses there is a broad distribution of sites for the guest ions, amounting to something like 50 different microenvironments in borosilicate hosts for example.[18] From the fluorescence line narrowing and the temperature dependence of the bandwidths plus the EPR data of Iton et al.,[15,16] we assert that the line widths observed in Figure 1 are due to inhomogeneous broadening. This is probably a manifestation of the poor long-range order in the zeolite caused by (i) partial occupancy of available sites, (ii) imperfect silicon–aluminum ordering, (iii) the presence of hydroxyl and/or oxo groups, (iv) residual sodium ions occupying sites in both the α and β cages, (v) dealumination during dehydration, and (vi) the presence of residual water molecules either from incomplete dehydration or adsorbed from the vacuum system.

It is instructive at this point to consider the possible site symmetries of the europium ions in dehydrated zeolite Y. A good indication of the major types of site occupied by the rare-earth ions is provided by the far-infrared spectrum of this material (Figure 4A). The frequencies of the vibrational modes in the far-infrared spectrum are useful indicators of cation type and site symmetry[8] and for rare-earth ions, the cation–oxygen stretching vibrations are anticipated to occur below 200 cm^{-1} analogous to the data of Nelson and Exarhos[24] showing far-IR absorptions due to europium cations in phosphate glasses. In Figure 4A, accompanying a weak band at 200 cm^{-1} due to residual sodium ions located in the supercage at site II, there are three major absorption bands due to the rare-earth ions. These reflect occupancy of both the α and β cages by europium ions. Although there is no neutron diffraction or X-ray crystal structure available in the open literature of any Y type zeolite containing europium ions, in concert with other rare-earth Y zeolites,[25-27] the three major sites occupied are probably II, I, and I'. Comparing the vibrational spectra to those observed previously for other Y zeolites,[8] it is sensible to retain the frequency ordering of the absorptions caused by cations in these sites. Therefore, as before the expected frequency ordering is II > I > I' as shown on the figure. It should be noted here that the apparent intensity of the rare earth cation vibrations are low compared to that of the residual sodium ions. This is due to the reciprocal relationship between the cation mass and the infrared intensity.[8] Thus, besides the threefold decrease in far-IR band area due to a population effect, there is an additional factor of 6.5 due to the mass of the europium ion. Therefore the europium ion vibrational bands appear almost 20 times weaker than the corresponding sodium cation vibrations.

Although the crystal field splittings for f orbitals are much smaller than those observed for d orbitals, there is no evidence that any of the bands observed in the far-IR are due to electronic transitions.[33] In this case the lowest energy transition would occur from the $J = 0$ level to the $J = 1$. The energy of this transition

(18) Rice, D. K.; DeShazer, L. G. *Phys. Rev. B* **1969**, *186*, 387.
(19) Reisfeld, R. *J. Electrochem. Soc.* **1984**, *131*, 1360.
(20) Durville, F. D.; Boulon, G.; Reisfeld, R.; Mack, H.; Jorgenson, C. K. *Chem. Phys. Lett.* **1983**, *102*, 393.
(21) Reisfeld, R. *Struct. Bonding (Berlin)* **1979**, *30*, 65. Blasse, G. *Solid State Chem.* **1982**, *3*, 153.
(22) Selzer, P. M.; Huber, D. L.; Barnett, B. B.; Yen, Y. M. *Phys. Rev. B* **1978**, *17*, 4979.
(23) Brecher, C.; Riseberg, L. A. *Phys. Rev. B* **1976**, *13*, 81.
(24) Nelson, B. N.; Exarhos, G. J. *J. Chem. Phys.* **1979**, *71*, 2739.
(25) Bennett, J. M.; Smith, J. V. *Mater. Res. Bull.* **1969**, *4*, 77.
(26) Smith, J. V.; Bennett, J. M.; Flanigen, E. M. *Nature (London)* **1967**, *215*, 241.
(27) Gallezot, P.; Imelik, B. *J. Chim. Phys.-Physchem. Biol.* **1971**, *68*, 34.
(28) Baker, M. D.; Ozin, G. A., unpublished results.
(29) Stein, G.; Wurzberg, E. *J. Chem. Phys.* **1975**, *62*, 208.
(30) Haas, Y.; Stein, G. *J. Phys. Chem.* **1971**, *75*, 3677.
(31) DeWilde, W.; Peeters, G.; Lunsford, J. *J. Phys. Chem.* **1980**, *84*, 2306.
(32) Suib, S. L.; Bordeianu, O. G.; McMahon, K. C.; Psaros, D., In *Inorganic Reactions in Organized Media*; Holt, S. L., Ed.; ACS Symp. Ser. 177; American Chemical Society: Washington, DC, 1982.
(33) Hadni, A. In *Far Infrared Properties of Solids*; Mitra, S. S., Nudleman, S., Eds.; (Proceedings of a NATO Advanced Study Institute held in Delft, The Netherlands, Aug 5–23, 1968).

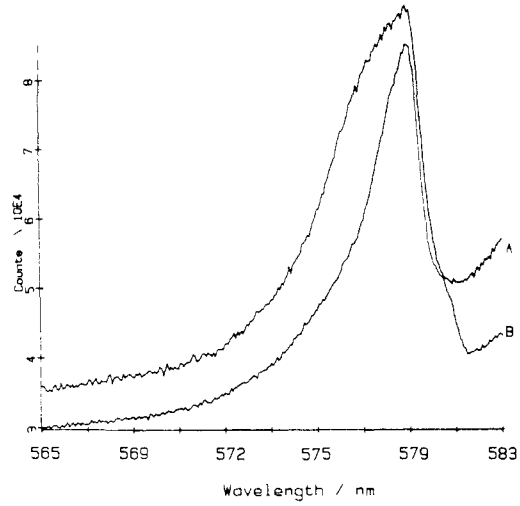

Figure 5. $^5D_0$ to $^7F_0$ emission from zeolite-entrapped Eu^{3+}: (A) dehydrated at 400 °C in vacuo; (B) oxidized at 400 °C under 300 Torr of oxygen. Note that the oxidation, as well as having the effect of increasing the fluorescence yield, also produces an increase in intensity of the high-frequency component (shoulder) of the band. The spectra have been arbitrarily scaled to have the same heights.

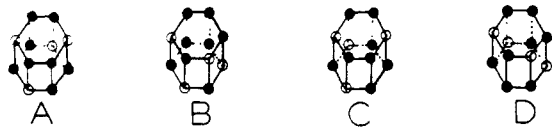

Figure 6. The possible site symmetries for Eu^{3+} ions located in site I: (A) D_2; (B) C_2; (C) C_s; (D) C_{2h}, where ● denotes Si and O denotes Al. Note that only B and C possess the correct symmetry to account for the observed spectra. The europium ions located within the hexagonal prisms have been omitted for clarity.

would be over 200 cm^{-1} (see Figure 1) and will therefore not interfere with the vibrational part of the far-infrared spectrum. Also the far-IR spectrum of La^{3+} zeolite Y is similar to that shown here for Eu^{3+} Zeolite Y,[28] reinforcing the proposal that the observed far-IR bands are rare earth cation modes as there will be no f–f transitions in the f^0 case.

Further information on the local site symmetry of the emitting europium ions can be discerned from Figure 1. The fact that the transition to the $J = 0$ level is observed indicates that the local symmetry is C_s, C_{nv}, or C_n. Further detail of this band is shown in Figure 5A. Since this emission band is the result of a transition between two $J = 0$ levels, it will not show any splittings due to crystal field effects. Thus any asymmetry in the band shape can be linked to emissions from europium ions in distinct environments. The shape of this band indicates at least two, and probably three, major crystallographic sites for the emitting centers. This is in general agreement with the far-IR observation of site II, I, and I′ europium ions, all of which can locate in the necessary symmetry for this transition to occur. Note, however, that this in fact places a considerable constraint on the europium ions that are detected by this technique. For example, in the case of site I ions, it is only those in C_2 and C_s symmetries that are observed. Those in local D_2 and C_{2h} sites are nonemitting and are therefore not detectable. (See, for example, Figure 6). Therefore the relative intensities of the components of the $J = 0$ emission band, unlike the far-IR absorption bands,[8] do not give reliable Eu^{3+} population information, unless the majority of the europium ions are in sites conducive to emission. An indication of the degree of asymmetry surrounding the emitting ions comes from an examination of the relative intensities of the observed transitions. These are assembled in Table I together with those observed for europium ion emission in various environments. Since the transition to the $J = 1$ level is a magnetic dipole phenomenon,[21] the intensity of this band is largely unaffected by the crystal field environment of the europium ion. It can therefore be taken as a standard to gauge the relative intensities of the other bands in the spectrum.[21] Since the electronic transitions of Eu^{3+} involving J changing by 2 are strongly dependent on the surrounding medium (hypersensitive transitions),[21] it is the ratio of the intensities of the hypersensitive to the magnetic dipole transition that carries the most information on the local symmetry around the emitting europium ion. The ratio of the intensities of these transitions in zeolite Y is seen to be close to those observed in silicate glasses at 4.38:1.[21] The local symmetry of the europium ion is therefore seen to be somewhat higher than in germanate and slightly lower than in phosphate glasses.

(B) Oxidized Form: Site Information. Following oxidation of the dehydrated zeolite at 400 °C, there were a number of pronounced changes in both the far-IR and fluorescence spectra of the zeolite. The changes in the far-IR vibrational profile of the europium cations are shown in Figure 4B. In general, the appearance of the spectrum remains the same, again signaling the occupation by europium ions of three major extraframework sites. However, the relative intensity of the site II band to that of the site I has changed, indicating a migration of rare-earth ions from the hexagonal prisms into the supercages. This effect seems to be prevalent in all the rare earth ion exchanged zeolites that we have studied and will be the subject of a subsequent paper.[28] We feel that this oxygen-induced transformation is not due to an oxidation state change of the europium ion for two reasons: (i) the concentration of Eu^{2+} in the dehydrated form is extremely small and was undetectable in the emission spectra[34] and (ii) the same transformation was oberved for Sm^{3+}-containing zeolite Y, and Sm^{4+} is not a stable oxidation state. In fact, studies of oxidation state changes of europium ions in various zeolites with dehydration, oxygen, and chlorine treatments have been previously reported using Mössbauer and EPR spectroscopy.[35] In this work, there was no evidence for reduction of Eu^{3+} to Eu^{2+} upon vacuum dehydration up to 600 °C.

The changes in the fluorescence spectrum following oxidation are shown in Figure 5B for the $J = 0$ transition. As previously described, the asymmetry of this band indicated two, and possibly three, major europium ion sites. Following oxidation there is a growth in the intensity of the high-energy side of this band. This is possibly a manifestation of the migration of europium ions from the hexagonal prisms to the supercages. One therefore tentatively assigns the higher energy component of this band to emissions from supercage Eu^{3+} ions.

In the oxidized form, the ratio of the $J = 1$ to $J = 2$ transition was essentially unchanged from that in the dehydrated form, although the hypersensitive emission band had changed shape. This indicates a small change in the local symmetry of the europium ions. Concomitant with the oxidation, there was a large increase in emission intensity. It is quite likely that the reason for this increase in intensity is due to the perturbation of quenching centers. This could be their complete removal from the vicinity of the emitting europium ions or possibly an increase in the distance between the rare-earth ion and the quenching center. These are probably hydroxyl groups, which are known to be effective quenchers of rare earth fluorescence[29,30] either as structural groups or located on the cations (hydrolyzed ions). Deuteriation studies, combined with controlled dehydroxylation experiments followed both by mid-IR and luminescence, are now under way to clarify this point.

Alternatively the increase in luminescent intensity can be linked to the oxygen-induced migration of the rare-earth ions from nonemissive or weakly emissive high-symmetry sites (e.g., site I) to lower symmetry highly emitting sites (site II). However, judging from the change in intensities of the far-IR absorptions due to cations in these sites, a fairly major reorganization has occurred. One would expect therefore a major change in the relative in-

(34) Arakawa, T.; Takuta, T.; Takakuwa, M.; Adachi, G.-Y.; Shiokawa, J. *Mater. Res. Bull.* **1982**, *17*, 171.
(35) Suib, S. L.; Zerger, R. P.; Stucky, G. D.; Emberson, R. M.; Debrunner, P. G.; Iton, L. E. *Inorg. Chem.* **1980**, *19*, 1858.
(36) McCann, W. A.; Rees, L. V. C. In *Proceedings of the Sixth International Zeolite Conference*, Reno, NV, July 1983.

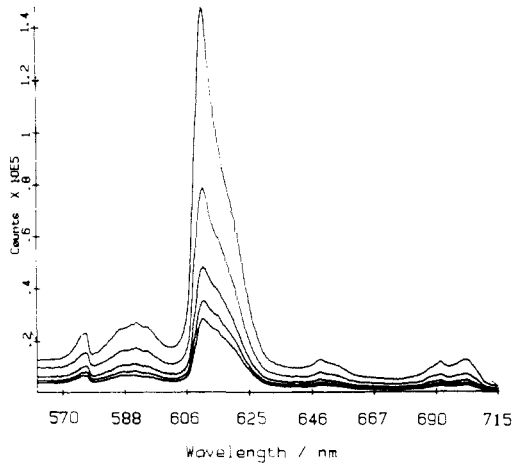

Figure 7. Quenching of Eu^{3+} zeolite Y luminescence by oxygen. Pressures in Torr: (a) vacuum; (b) 105; (c) 300; (d) 500; (e) 700. (a) Uppermost trace; (e) lowermost trace.

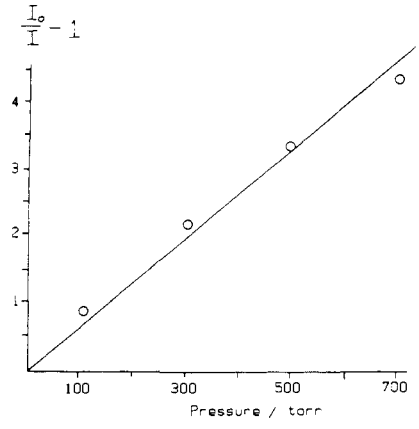

Figure 8. Stern–Volmer plot for the luminescence quenching depicted in Figure 7. The intensities were measured at the peak of the $J = 2$ transition (see Figure 1).

tensities of the magnetic dipole and hypersensitive transitions. This is not the case and indicates that the former mechanism involving perturbation of quenching centers is largely responsible for this effect.

(C) Gas-Phase Quenching of Europium Ion Fluorescence. The recognition of molecules entering the pore system of the zeolite by an optical response was the original goal of this study. This has important ramifications in fabricating a zeolite-based chemical sensor. Coupled with the size and shape molecular selectivity of these materials, an adsorbate-sensitive optical signal is highly desirable. In this section we describe the fluorescence quenching of Eu^{3+} ions in zeolite Y by adsorption of oxygen. In order to minimize the effect of small concentrations of divalent europium ions on the data, the experiments were carried out with the oxidized form of the zeolite.

The manner in which the intensity of the europium ion fluorescence is quenched is shown in Figure 7. Upon exposure of the zeolite to static pressures of oxygen, the luminescence intensity decreased. The quenching was rapid, was completely reversible, and showed no indication of the hindered diffusion of oxygen to the emitting sites. The quenching kinetics were Stern–Volmer in nature as shown in Figure 8 for the peak of the $J = 2$ transition. This is the first time that a single region of linearity has been observed for intrazeolitic luminescence quenching. In previous studies, Stern–Volmer plots for the intrazeolitic quencing of $Ru(bpy)_3^{2+}$ [31] and UO_2^{+} [32] have shown two linear regions, which has been explained in terms of the quenching of emitting species immobilized both on the external surface and in the interior of the zeolite. Since oxygen is a small molecule (kinetic diameter = 3.54 Å) and can easily diffuse through the

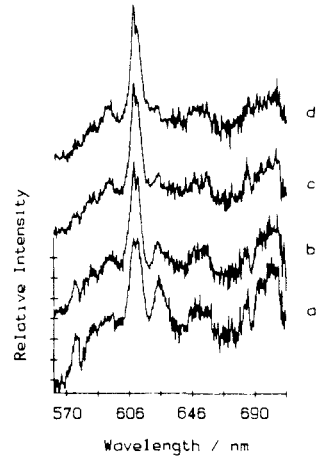

Figure 9. Ratio spectra from the quenching data of Figure 7: (a) a/b; (b) a/c; (c) a/d; (d) a/e. Note that the bands do not change at the same rate, indicating that the luminescent quenching is probably Eu^{3+} cation site selective (see text).

12 ring openings to the supercages of zeolite Y, this behavior is absent. The distinction therefore between surface and bulk europium ions by fluorescence quenching will only be possible with more bulky adsorbates, where diffusion is hindered by the pore size of the zeolite.

We note here that a linear plot of the luminescent lifetime decay constant has been reported for H_2O/D_2O quenching of europium(III) in zeolite Y.[5] In our studies, the temporal decay profile of the $^5D_0$ to $^7F_2$ emission also showed lifetime quenching with oxygen and a number of other adsorbates, for example, acetylacetone. A comparison of the quenching behavior of these adsorbates will be extremely interesting, and will be the subject of further study.[28] Indeed, in producing a selective chemical sensor, the recognition of discrete optical responses for different molecules is crucial.

From the data shown in Figure 7 there is evidence that the quenching is showing site selectivity. This can be better appreciated by examining the ratio spectra displayed in Figure 9. Here, the spectrum of the virgin zeolite (Figure 7a: no oxygen present in the gas phase) is divided by each of spectra b–e in Figure 7. If all the bands in the spectra were decreasing at the same rate, then the ratio spectra resulting from these divisions would be invariant. This is certainly not the case. Bands at 646 and 579 nm are definitely decreasing at a rate different from that, for example, at 612 nm. This luminescence intensity ratio technique therefore indicates the presence of at least two differently sited fluorescing europium ions that are quenched by oxygen at different rates. Conversely, the difference in the spectrum before and after the introduction of oxygen can be rationalized by the increased contribution to the spectra of an unquenched europium ion, for example, in site I. Ions in this site as discussed previously could well have a spectrum rather different from those in site II in the α cage. As the fluorescence of these accessible ions is progressively quenched, that from the inaccessible hexagonal prism ions shows a larger contribution to the observed spectrum.

4. Conclusions

In this paper we present the first far-infrared and laser-induced fluorescence spectra of ion-exchange europium zeolite Y. The spectra lead to the following conclusions.

1. The europium ions are located in many different microenvironments (glassy model) which cover three major sites (II, I, and I′).

2. Inhomogeneous line broadening contributes to the observed bandwidths of the europium ion far-IR cation modes and visible luminescence spectra.

3. The local symmetry of the rare-earth ion is low. From the luminescence spectra it is C_s, C_n, or C_{nv}.

4. Oxidation of the dehydrated sample induces a migration of the europium ions from the β to α cages.

5. The europium ion fluorescence is effectively quenched by molecular oxygen following Stern-Volmer kinetics.

Acknowledgment. The generous financial assistance of the Natural Science and Engineering Research Council of Canada's Operating and Strategic Grants Programmes and the Connaught Foundation of the University of Toronto is greatly appreciated. We are also indebted to Dr. Edith Flanigen (Union Carbide) for supplying various high-crystallinity and ultrahigh-purity FAU zeolites as well as invaluable technical discussions.

Registry No. Eu^{3+}, 22541-18-0; $EuCl_3$, 10025-76-0; O_2, 7782-44-7.

Synthesis and Electrochemistry of $(CO)_2(PMe_3)Fe(\mu_2\text{-}t\text{-}Bu_2P)(\mu_2\text{-}CO)Rh(PMe_3)L$(*Fe–Rh*) (L = CO, PMe_3). Digital Simulation of Modified ECE Mechanism. X-ray Crystal Structures of $(CO)_2(PMe_3)Fe(\mu_2\text{-}t\text{-}Bu_2P)(\mu_2\text{-}CO)Rh(PMe_3)_2$ and $[Me_3PO{\cdot}Na(15\text{-crown-}5)]^+[(CO)_3Fe(\mu_2\text{-}t\text{-}Bu_2P)Rh(PMe_3)(CO)]^-$

Roger D. Moulton, Don J. Chandler, Atta M. Arif, Richard A. Jones,* and Allen J. Bard*

Contribution from the Department of Chemistry, The University of Texas at Austin, Austin, Texas 78712. *Received August 14, 1987*

Abstract: Reaction of the lithiated iron phosphine complex $Fe(CO)_3(t\text{-}Bu_2PH)(t\text{-}Bu_2PLi)$ with $(Rh(CO)_2Cl)_2$ or $Rh(PMe_3)_3Cl$ in THF yields the heterobimetallic phosphido bridged complexes $(CO)_3(t\text{-}Bu_2PH)Fe(\mu_2\text{-}t\text{-}Bu_2P)Rh(CO)_2$ (**1**) and $(CO)_2(PMe_3)Fe(\mu_2\text{-}t\text{-}Bu_2P)(\mu_2\text{-}CO)Rh(PMe_3)_2$ (**2**), respectively. **2** can also be prepared from $(CO)_2(t\text{-}Bu_2PH)Fe(\mu_2\text{-}t\text{-}Bu_2P)(\mu_2\text{-}CO)Rh(COD)$ and excess PMe_3 (COD = 1,5-cyclooctadiene). Reaction of **1** with PMe_3 or **2** with CO (1 atm) yields $(CO)_3(PMe_3)Fe(\mu_2\text{-}t\text{-}Bu_2P)Rh(CO)(PMe_3)$ (**3**). Both **2** and **3** may be reduced with Na sand to radical anions, and the reduction of **3** in the presence of 15-crown-5 and traces of O_2 led to the isolation of $[(15\text{-crown-}5)Na(Me_3P{=}O)]^+[(CO)_3Fe(\mu_2\text{-}t\text{-}Bu_2P)Rh(CO)(PMe_3)]^-$ (**4**). The molecular structures of **2** and **4** have been determined via single-crystal X-ray diffraction studies. The molecular geometries of both complexes contain a di-*tert*-butylphosphido unit which spans a single Fe–Rh bond. In **2** the Fe atom is six coordinate if one includes the Fe–Rh bond. If one excludes the Fe–Rh bond the geometry about Fe may be considered to be trigonal bipyramidal. The Rh atom in **2** is five coordinate, including the Fe–Rh bond. The geometry about Rh is best described as a square-based pyramid with the carbon atom of the bridging CO unit occupying the vertex. In **4** the coordination geometry about Fe is trigonal bipyramidal and about Rh it is roughly square planar including the Fe–Rh bond in both cases. The molecular geometry of **3** is similar to that of **2** based on spectroscopic evidence. Cyclic voltammetry of **2** and **3** shows two oxidation waves and an irreversible two-electron reduction wave. The product of the reduction is oxidized in a reversible 1 e^- process to an anion radical that can be further oxidized to reform the original compound. A third oxidation at low scan rates or at high concentrations is also seen. Digital simulations of the voltammetry show this wave corresponds to a dianion species formed by a disproportionation reaction in solution. Possible structures of the electrochemically produced species are proposed. X-ray crystal data for **2** ($C_{20}H_{45}FeO_3P_4Rh$): M = 616.23, monoclinic, $P2_1$, (No. 4), a = 10.719 (2) Å, b = 10.148 (3) Å, c = 13.637 (3) Å, β = 95.63 (2)°, U = 1476.1 (5) Å^3, D_c = 1.386 g cm^{-3}, Z = 2, μ(Mo Kα) = 12.72 cm^{-1}. Refinement of 1756 reflections ($I > 3\sigma(I)$) out of 2756 unique observed reflections ($2° < 2\theta < 50°$) gave R and R_w values of 0.054 and 0.059, respectively. Crystal data for **4** ($C_{28}H_{56}FeNaO_{10}P_3Rh$): M = 826.97, monoclinic, $P2_1/c$, (No. 14), a = 12.246 (3) Å, b = 10.688 (5) Å, c = 31.326 (5) Å, β = 94.63 (2)°, U = 4087.0 (5) Å^3, D_c = 1.142 g cm^{-3}, Z = 4, μ(Mo Kα) = 9.17 cm^{-1}. Refinement of 1670 unique observed reflections ($3° < 2\theta < 48°$) gave R and R_w values of 0.087 and 0.096, respectively. Common to both structures: λ(Mo Kα) = 0.71073 Å, graphite monochromator. MULTAN, difference Fourier, and full-matrix least squares were the methods used.

Electrochemical investigations of bimetallic organometallic complexes often demonstrate that conformational changes and isomerizations occur prior to and following electron transfer.[1] Electrochemistry thus serves as a probe into the reactivity and stability of complexes in new oxidation states. For example, electrochemistry has been applied to the study of the effect of the electron transfer on the metal–metal interaction.[2] Reduction of a dinuclear species tends to decrease the metal–metal bond order, whereas oxidation tends to increase it. If the metal–metal bond is disrupted following electron transfer, the presence of a bridging group may help to maintain the integrity of the complex. Geometric isomerization or bonding rearrangements in the coordination sphere may also occur following reduction or oxidation, especially with complexes in which bonds are strained. Thus, there has been considerable interest in the study of reactions that accompany electron transfer, and the effect these have on the observed electrochemistry.

We have been investigating the effect of structure of bimetallic systems on homogeneous reactivity[3] and on the redox processes

(1) (a) Kolz, J. C. In *Topics in Organic Electrochemistry*; Fry, A. J., Britton, W. E., Eds.; Plenum: New York, 1986; p 83 and references therein. (b) Evans, D. H.; O'Connell, K. M. In *Electroanalytical Chemistry*; Bard, A. J., Ed.; Marcel Dekker: New York, 1986; Vol. 14, p 113.

(2) Roberts, D. A.; Geoffroy, G. L. *Comprehensive Organometallic Chemistry*; Wilkinson, G., Stone, F. G. A., Abel, E. W., Eds.; Pergamon: New York, 1982; Vol. 6, Chapter 40.

(3) (a) Chandler, D. J.; Jones, R. A.; Stuart, A. L.; Wright, T. C. *Organometallics* **1984**, *3*, 1830. (b) Jones, R. A.; Wright, T. C. *Organometallics* **1983**, *2*, 1842. (c) Alta, A. M.; Chandler, D. J.; Jones, R. A. *Organometallics* **1987**, *6*, 506. (d) Chandler, D. J. Ph.D. dissertation, The University of Texas, 1986, and references therein. (e) Arif, A. M.; Heaton, D. E.; Jones, R. A.; Kidd, K. B.; Wright, T. C.; Whittlesey, B. R.; Atwood, J. L.; Hunter, W. E.; Zhang, H. *Inorg. Chem.* **1987**, *26*, 4065.

0002-7863/88/1510-5714$01.50/0 © 1988 American Chemical Society